Multilayer coatings for x-ray mirrors: extraction of stack parameters from x-ray reflectivity scans and comparison with transmission electron microscopy results

Daniele Spiga
Giovanni Pareschi
Vincenzo Cotroneo
Rodolfo Canestrari
Dervis Vernani
INAF/Osservatorio Astronomico di Brera
Via Bianchi 46
23807 Merate (LC), Italy
E-mail: daniele.spiga@brera.inaf.it

Alessandro Mirone
Claudio Ferrero
European Synchrotron Radiation Facility (ESRF)
6 rue J. Horowitz
BP 220
38043 Grenoble, France
E-mail: ferrero@esrf.fr

Claudio Ferrari
Laura Lazzarini
IMEM-CNR
Parco Area delle Scienze 37/A
43010 Fontanini-Parma, Italy
E-mail: ferrari@imem.cnr.it

Abstract. The reflectance effectiveness of a multilayer depends strongly on the stack properties (thickness, roughness, and density of each layer) and can be directly tested by means of x-ray reflectivity scans at definite photon energies. The reflectivity curves are also a powerful tool for the in-depth, nondestructive characterization of the stack structure: The complex task of extracting the stack parameters from reflectivity curves can be achieved via a suitable best-fitting computer code based on a global automatic optimization procedure. We present the computer-assisted layer-by-layer analysis of the characteristics of Ni/C, Pt/C, and W/Si multilayers, based on x-ray reflectivity scans performed at 8.05 and 17.45 keV. In order to verify the correctness of the code predictions, we present also a comparison of the computer model with the transmission electron microscope profiles of the same multilayer samples.
[DOI: 10.1117/1.2769325]

Subject terms: x-ray multilayers; x-ray reflectivity scan; automatic fitting procedure.

Paper 060690R received Sep. 1, 2006; revised manuscript received Jan. 18, 2007; accepted for publication Feb. 6, 2007; published online Aug. 7, 2007. This paper is a revision of a paper presented at the SPIE conference on Space Telescopes and Instrumentation II: Ultraviolet to Gamma Ray, May 2006, Orlando, Florida. The paper presented there appears (unrefereed) in SPIE Proceedings Vol. 6266.

1 Introduction

Multilayer coatings with periods in the nanometer range have proven to provide a suitable technological base for enhancing the reflectance of extreme ultraviolet (EUV), neutron, and x-ray mirrors at incidence angles larger than the critical one. Nowadays, multilayer-coated mirrors are standard components of many synchrotron beamlines to deviate, concentrate, and filter intense x-ray beams. Ni/Ti multilayers are used in neutron optics. The next generation of nanometer-sized electronic components may be manufactured by EUV lithography, which requires also Mo/Si multilayer-coated mirrors in order to concentrate EUV radiation efficiently in normal incidence. Moreover, the adoption of wideband graded multilayer coatings is foreseen for the production of x-ray optics for future x-ray telescopes (HEXIT-SAT,[1] Con-X,[2] XEUS,[3] SIMBOL-X,[4] etc.) in order to extend their reflectivity bandwidths to the hard x-ray band (from 10 keV up to 70 to 80 keV) at grazing incidence angles of 0.2 to 1 deg. This approach has already been followed in previous works.[5,6]

A great effort is currently being made to develop multilayers with high reflectance over selected neutron, EUV, and x-ray energy bands. Several methods can be applied to deposit multilayer coatings, such as e-beam evaporation, ion-assisted deposition, ion-etched deposition, DC or RF magnetron sputtering, or ion-beam sputtering. Optimization processes are needed for each specific application. Analogous considerations hold as well for the multilayer structures, which should be designed according to the required reflectance as a function of energy. However, the reflection effectiveness depends crucially on the thickness precision of each layer and the interfacial roughness, which must be kept as low as possible. Therefore, in order for the multilayer coating technology to progress, a tool is needed to systematically assess the quality of test samples (uniformity, smoothness, and correct layer thickness in the stack). Transmission electron microscope (TEM) images allow a direct, quantitative evaluation of the layer thickness, but due to the long, complex sample preparation procedure and the subsequent sample destruction, this method can be used only for a limited number of samples.

X-ray reflectivity (XRR) measurements performed at a fixed energy for varying incidence angles can be routinely performed to inspect large numbers of samples. The fine interferential features of XRR curves reflect very precisely the deep multilayer stack structure. This causes XRR to be a very powerful diagnostic tool for multilayer stacks, or any

0091-3286/2007/$25.00 © 2007 SPIE

other layered structure with typical period in the nanometer range. Moreover, it is nondestructive and quick, and it does not require any particular sample preparation. Finally, it is sensitive not only to TEM-visible properties (thickness, interdiffusion, crystallization state), but also to other properties (layer density, high-frequency microroughness) that cannot be measured by TEM.

On the other hand, the complexity of the dependence of XRR scan features on all the individual thickness, density, and roughness values in the stack makes the interpretation of XRR data difficult. The recursive[7] or matrix[8] formalism (including the consideration of microroughness via a modification[9] of the Fresnel coefficients or the Nevot-Croce approach[10]) may be used as a suitable basis for the model fitting of experimental curves: indeed, the exact XRR curve simulation would require reproducing *all* the thickness irregularities in an N-bilayer stack, involving a manual adjusting of more than $4N$ independent parameters, including the thickness and roughness of each layer. Moreover, a well-known problem of multiparameter fitting is that correlated parameters (e.g., the density and the roughness of the layers) can have similar effects on the XRR curves: therefore, the solution can be nonunique because a fit can result from different combinations of values of correlated parameters.

Nevertheless, the very large number of parameters characterizing a multilayer can be handled by computer programs: several codes to fit multilayer reflectivity curves—like IMD, which is included in the XOP package,[11,12]—have been written over the years. The effectiveness of the fitting algorithm depends on its ability to converge at a high rate to the best global fit of the XRR model to the experimental curve. Some codes make use of genetic algorithms[13–15] to reduce the risk of convergence to a local minimum. Other programs, conceived for similar tasks, perform a global minimization via an iterative simplex procedure,[16] or make use of other minimization techniques to refine thickness profiles obtained through analytical methods.[17]

In this work we have used Pythonic Program for Multilayers (PPM) to model-fit x-ray multilayer reflectivity curves. PPM, developed by one of us (A. Mirone, ESRF), performs a fast multiparameter constrained optimization of the reflectivity scans at one or more energies at the same time, using a very efficient, global minimization routine. It should be noted that the simultaneous fit at more than one energy helps to separate the variations of correlated parameters (e.g., density and roughness), because they generally change the reflectivity curves according to different dependences on the energy. Thus, PPM should play an important role in the diagnosis of nanometer-layered structures by XRR analysis. PPM has already been successfully used at the ESRF to determine the optical constants of uranium by fitting U/Fe multilayer XRR data.[18]

In this paper we show the XRR analysis of Pt/C, Ni/C, and W/Si multilayer samples at two standard energies, 8.05 keV (Cu Kα_1 line) and 17.45 keV (Mo Kα line), performed at INAF/Osservatorio Astronomico di Brera (Milan, Italy). The PPM program has been successfully used to perform a layer-by-layer analysis of reflectivity curves. Moreover, in this work we deal with an interesting comparison of the results of PPM with the TEM images of the same samples produced at the IMEM-CNR Institute (Parma, Italy). A brief description of PPM is given in Sec. 2. In Sec. 3 we describe our XRR setup and the reflectivity curves of the analyzed multilayer samples. In Sec. 4 we show the PPM results and compare them with the TEM findings; remarkable agreement of the two methods will be apparent from the comparison. The XRR analysis, moreover, proves not to be affected by artifacts that can alter the TEM images of multilayer coating sections. The fit results are briefly discussed in Sec. 5.

2 The PPM Computer Program

An in-depth analysis of the structure of the investigated multilayer samples has been performed, letting the fit parameters vary independently for each layer or for groups of layers of the stack, using PPM. This program, written in Python and C, is specifically conceived for the fast determination of the stack parameters by fitting reflectivity curves accurately; this allows one to take into account also the reflectance features caused by the deepest layers. The program reads in the files of reflectivity curves and a file defining the structural arrangement to be optimized. The number of free parameters may vary according to the supposed complexity of the stack. For example, one can assume each layer thickness to be a free variable, or instead one can assume a gradual drift of the layer thicknesses. Analogous considerations hold for layer densities and rms roughness. Finally, the user must also enter the lower and the upper limits as well as an initial guess for each defined variable.

Starting from the initial values, PPM computes the reflectivity curve R_c for each available experimental scan R_m, using the following figure of merit (FOM),

$$\mathrm{FOM} = \sum_i \left|\log R_m(i) - \log R_c(i)\right|,$$

where i is the index corresponding to the i'th angular point. The minimization algorithm varies the selected parameters within the bounds fixed by the user. It is well known that a logarithmic FOM assigns larger weights to smaller reflectivity values; hence one can recover important information on the reflectance of the deeper layers. Additional weights can be set in the FOM definition in order to restrict the fitting to particular sections of the XRR scan. Other kinds of FOM could also be adopted, e.g. the mean squared difference of the logarithms[13,14]; the one we adopted is preferable because it causes the fit to be less sensitive to the experimental errors caused by the instrumental noise.[13]

The adopted algorithm is a variant of the well-known downhill simplex[19] (or amoeba) algorithm. A set of $N+1$ points in an N-dimensional parameter space follows a series of movements converging to the nearest minimum. However, the downhill simplex alone would very likely stick at a local minimum. For this reason an annealing mechanism,[20–22] which is able to trigger a jump out of a local minimum, is implemented. This procedure was already implemented in another program for the analysis and optimization of graded multilayers at the ESRF.[23]

The simulated annealing function associates a microscopic energy state of N particles to every point of the parameter space; the convergence to a local minimum is

compared to a thermalization process, leading to a state of definite temperature T. The system of particles is assumed to follow the Boltzmann energy distribution, where the FOM (depending on the current particle state) plays the role of the energy. With the classical downhill simplex algorithm, moves increasing the FOM would be always excluded. If the system stabilizes according to the Boltzmann distribution at a large enough T, there is a nonzero probability that the system leaves the local minimum. Usually the initial T is set at a sufficiently high value in order to allow for a large number of transitions increasing the FOM, and while the system reaches the equilibrium, T is being slowly decreased.

As T is decreased, the probability of increasing the FOM during a transition gets lower and lower. At this point the system tends to converge towards the global minimum, till a minimum T value is reached, where the calculation stops. Thus, the probability of finding the global minimum is increased, since a much larger portion of the parameter space can be explored, at the expense of an increase in the computing time (with respect to the downhill simplex case).

The annealing procedure has also some critical aspects, such as the choice of the initial T and the cooling rate (usually an exponential decrease is adopted). A very slow cooling rate gives a greater degree of confidence that the global minimum has been found. These parameters as well as the multilayer structure and the initial parameter values have also to be carefully chosen in every single case.

The reflectivity fitting can work with a large number of free parameters, searching for the combination of values representing arguably the best possible fit of the scan. Once PPM has found a set of values that returns a model reflectivity curve agreeing well with the experimental one, we can be reasonably confident that this set represents a good approximation to the multilayer structure.

3 Experimental

3.1 *X-Ray Reflectivity Setup*

For our analysis we have focused on almost periodic multilayer samples deposited over flat Si wafers (4-in. diameter, 0.65-mm thickness, $\sigma_{\mathrm{rms}} \approx 3$ Å). The multilayer reflectivity was measured using a triple-axis Bede-D1 diffractometer (Bede Scientific Instruments Ltd, Durham, UK). A sealed x-ray tube with a Cu (or Mo) anode is used as a radiation source. For a detailed characterization of stack structures with a total thickness $D \approx 0.2$ μm using x rays of wavelength $\lambda \approx 1$ Å, a monochromatic beam ($\Delta E/E < 10^{-3}$), and a good angular resolution ($\Delta\vartheta < \lambda/2D \approx 25$ arcsec) over a wide angular range are required. The incident x-ray beam has therefore to be intense, collimated, and very thin in order to be entirely collected by the sample at very small incidence angles ($\vartheta_i \geqslant 500$ arcsec). In our experimental setup, in order to obtain a monochromatic collimated beam, a channel-cut Si crystal monochromator and a two-slit collimator have been taken. The x rays are dispersed by the crystal in directions depending on their energy: the diffracted beam, corresponding to the Kα line, is selected by the first slit (50 μm wide) at the exit of the Si crystal. Its divergence is $\approx$20 arcsec. A second slit (40 μm wide, just before the sample) reduces the lateral beam width to 70 μm; thus we are able to collect entirely the incident x-ray beam with 4-in. samples at incidence angles larger than $\approx$200 arcsec. The energy resolution $\Delta E/E$ is close to 10^{-4} when the Cu Kα_1 line is selected (for Mo Kα we cannot resolve the doublet, and the energy resolution is 5×10^{-4}) with a maximum counting rate of 10^5 count/s (10^4 count/s for Mo Kα). The incoming and the reflected beam are collected through an 800-μm-wide slit by a scintillator (photon counter) coupled to a photomultiplier with a pulse-height discriminator that limits the intrinsic background to <0.2 count/s. The scintillator is highly linear in the given flux operational range. The counts of the reflected photons were measured within an angular range between 0 and several thousand arcseconds in steps of 20 arcsec. The reflectance is then computed by normalization to the incident flux.

3.2 *Experimental XRR Curves*

The XRR scans show clear evidence of an irregular d-spacing variation along the stack. The initial values of the average stack parameters—namely, the average period, Γ factor [(heavier-element thickness)/(d-spacing ratio)], and rms roughness σ—were derived from a manual XRR simulation assuming a stack structure described by a small number of parameters. The preliminarily simulated XRR curves shown in Fig. 1 were traced using the simulation routines of the IMD package.

The first sample investigated is a Ni/C multilayer (19 bilayers) deposited at Media Lario Technologies (Bosisio Parini, Italy) by e-beam evaporation with the same facility used to deposit the single Au reflective coating of the SAX,[24] XMM,[25] and SWIFT-XRT[26] optics. The reflectivity curves at 8.05 keV (Fig. 1) and 17.45 keV were already reported and analyzed by some of us in previous works.[27,28] An interesting experimental result is the very high top reflectivity value of the first Bragg peak (95% at 8.05 keV), a world record[29] until 2005, just recently outdone.[30]

A laborious manual adjustment of parameters was necessary to bring the simulated reflectivity angular scans into preliminary agreement with the experimental data, even though small reflectance features (e.g., the fine structure of reflection minima) were not fitted by the assumed model. The matching of manual fit to experiment suggests that there could be a d-spacing drift in the stack of about 2 nm across the 19 bilayers, probably to be ascribed to C layers. The derived average period is 13 nm. The Ni layers' thickness is approximately 3 nm. An interesting result is the value inferred for the C density (1.6 g/cm^3), which is lower than that of natural C (1.8 to 2.5 g/cm^3 for amorphous carbon); such a low value for evaporated C films has already been reported in the literature.[31] Nickel has instead been found to be deposited at densities (8.7 g/cm^3) near the natural value (8.9 g/cm^3). Finally, the rms roughness is 4 Å with the actually found C density (3 Å if one assumes the natural density value), a value similar to that of the Si wafer substrate (3 Å).

The second sample is a Pt/C multilayer (15 bilayers) deposited by e-beam evaporation on a Si wafer: this sample is the result of a deposition test by INAF/OAB and Media Lario Technologies to calibrate the deposition facility before producing a hard-x-ray optic prototype.[32] Also in this case the peak reflectivity is high (74% at 8.05 keV; see Fig.

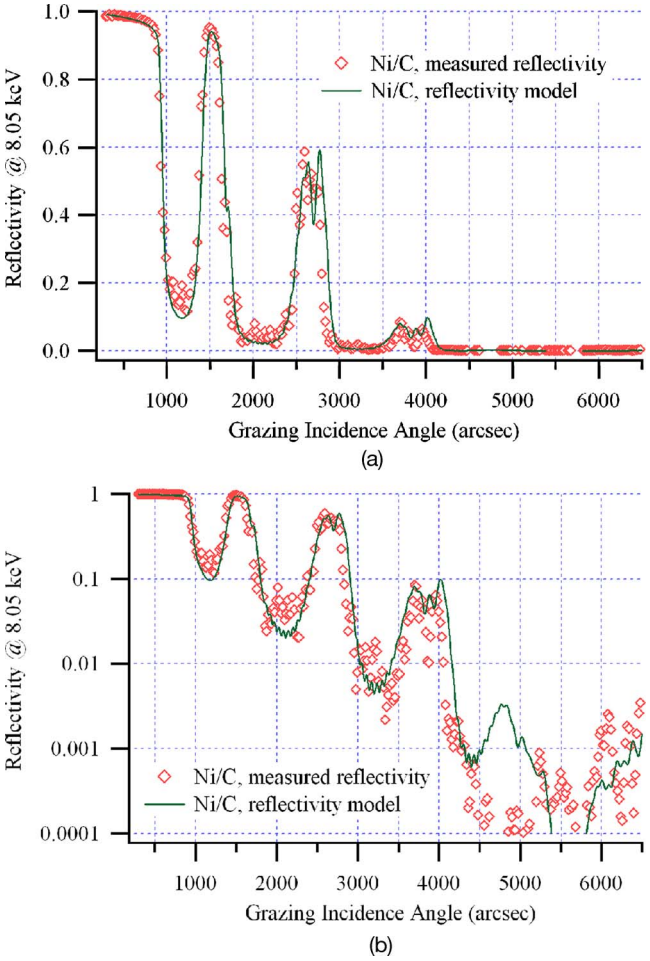

Fig. 1 XRR curves (plotted points) at 8.05 keV referring to the Ni/C multilayer sample with 19 bilayers: (a) linear and (b) logarithmic scale. A preliminary model with manually derived parameters (the solid line) appears to match the experiment well on a linear scale, but actually the reflectance details are poorly reproduced, as can be seen on the logarithmic scale.

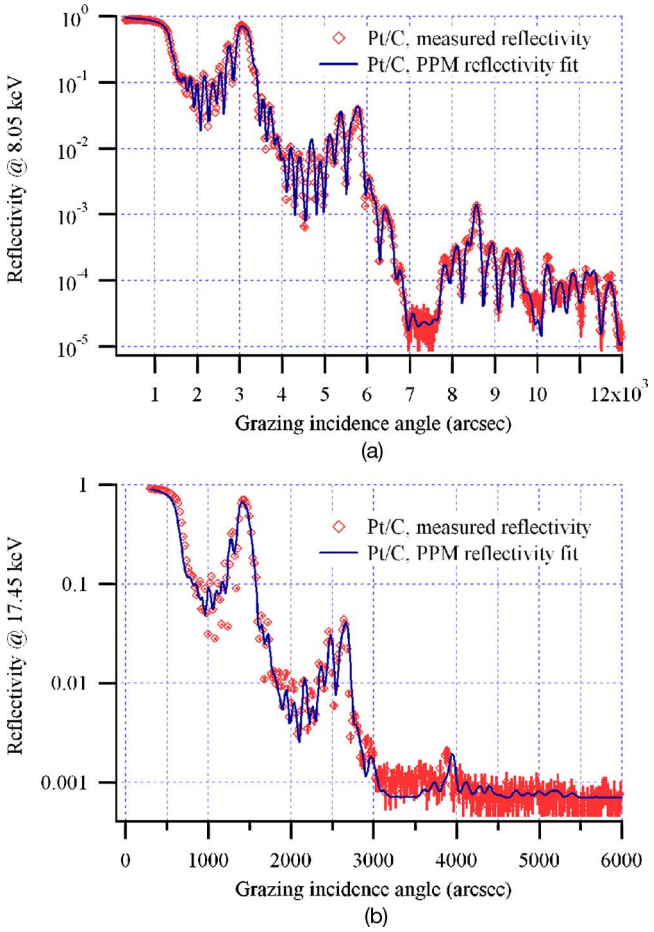

Fig. 2 The reflectivity (a) at 8.05 keV and (b) at 17.45 keV of the Pt/C multilayer sample compared with the fitting model calculated via PPM (log scale). The fit procedure was run simultaneously on both scans. The error bars (very small) are also included.

2). From the manual XRR modeling we inferred a 56-Å average d spacing, and a Γ factor around 0.42, but we could not simulate the complex structure of the peaks.

The third sample is a W/Si multilayer with 40 bilayers, deposited by DC magnetron sputtering on a Si wafer substrate. This sample was provided in 2004 by Reflex s.r.o. (Prague, Czech Republic): the variation of d spacing was due to the fact that the deposition process was not yet optimized at that time. The following optimization of the process allowed, indeed, the deposition of W/Si multilayers with excellent periodicity and smoothness.

From a manual fit of the third sample XRR (Fig. 8) we derived an average d spacing of 55 Å and a Γ factor of 0.17. However, most of the reflectance features could not be explained.

3.3 *TEM Measurements*

The TEM images were taken on the cross sections of the examined samples, making use of the amplitude contrast technique with a JEOL model 2000 FX TEM. In the section images the high-Z element (Pt, Ni, W) appears black and the low-Z element (C, Si) appears gray or white. The interfaces can be located where the gray or white turns to black, with an uncertainty of 3 Å (for interdiffusion-free multilayers); therefore the intrinsic error of a thickness measurement can be estimated to be around $\sqrt{2}\times 3$ Å$=4.2$ Å. In the following we report the layer thickness measurements with errors taken to be the quadratic sum of the intrinsic error and the uncertainty that can be caused by the local undulation of the interfaces.

4 Results of PPM Analysis

The multilayer stack structures of samples referred to in Sec. 3 have been analyzed by means of PPM. The structure assumed to carry out the fit varies according to the supposed complexity of the stack, and is described separately in each case; as an initial guess we always assumed a constant-d-spacing multilayer, matching the reflectance peaks to the primary peaks of the experimental reflectivity. The calculations were first performed assigning data weights proportional to the reflectance values, in order to fit the position and shape of the primary Bragg peaks. The derived values were then used as initial guesses for the final calculation, with no weights. Moreover, in order to refine the fit, the program needed to be restarted a few times,

always using the values found in the previous run as initial points, until a stable solution was found. PPM was run in a Linux environment with an AMD Sempron64 3400 processor (2 GHz). Some preliminary results obtained by PPM had already been reported elsewhere.[33,34]

4.1 Pt/C *Sample*

The Pt/C (15 bilayers) multilayer reflectivity curves at 8.05 and 17.45 keV were best-fitted simultaneously, letting the thicknesses of all layers be free to vary along the intervals 15 to 40 Å for Pt and 20 to 80 Å for C. The initial values were 23 Å for Pt and 33 Å for C. These very broad domains allow the exploration of a very wide range of solutions. Only the very first C layer, deposited directly on the substrate, has been ignored, since its presence does not noticeably affect the reflectivity profile. The rms roughness values for Pt and C were assumed to be constant in the stack, with different values comprised in the interval 2 to 6 Å. The densities were fixed to values lower than the bulk densities (Pt: 20.5 versus 21.5 g/cm^3; C: 1.6 versus 1.8 to 2.5 g/cm^3) as already found experimentally for samples deposited by e-beam evaporation (see also Sec. 3.2).

The whole calculation required approximately 1 h and 40 min. The final result matches the measured data very well both at 8.05 keV [see Fig. 2(a)] and 17.45 keV [see Fig. 2(b)]. The logarithmic χ^2 amounts to 5.67 at 8.05 keV and 4.45 at 17.45 keV. We carried out a test of fit significance by evaluating at both photon energies χ^2_ν, the reduced logarithmic χ^2 (i.e., $\chi^2_\nu=\chi^2/(M-P)$, with M the number of points in the experimental scan and P the number of fit parameters), and verifying that the two values are $\ll 1$. The value of χ^2_ν was found to be 0.010 at 8.05 keV and 0.014 at 17.45 keV; therefore the fit is significant at both energies.

The structure found is shown in Fig. 3(a). The aperiodicity comes mostly from the C layers, with evident oscillations around 35 Å, and a peak at 75 Å corresponding to the third deposited C layer. Pt layers are more constant, varying about 22 Å. It is worthwhile remembering that this result was found by assuming a regular, periodic multilayer as an initial guess. The calculated rms roughness values are 5.3 Å for Pt and 4.2 Å for C.

The verification of the PPM results through sample TEM sections confirms at a glance the presence of an exceptionally thick C layer at the expected position [the big bright band in Fig. 3(b)]. For a more detailed comparison, we extracted and compared individual Pt and C thicknesses obtained from TEM images and the PPM analysis. The thicknesses worked out from TEM profiles can however be affected by a significant error, brought in by the superposition of rough Pt profiles on the image plane, causing the Pt layers to appear thicker at the expense of the C layers. The shading effect is larger if the TEM sample is thicker, because a larger number of profiles are projected on the TEM image. This is easily seen in Fig. 3(b): near the sample edge, where the sample is very thin, the Pt layers are thinner than the C layers, whereas this ratio appears to be inverted far from the edge, where the TEM sample is thicker. In this area the Pt layers look denser and thicker while the C layers appear to be reduced by the same amount.

Because multilayer reflection results from multiple interference events of x rays at the *mean* interface of each Pt/C and C/Pt couple, the "true" thickness values which can be compared with those derived from XRR analysis should be measured where the TEM sample is very thin, i.e., where the overlapping of roughness profiles is negligible. Unfortunately, the sample edge line is not parallel to the growth direction, and a direct extraction of the true Pt layer thickness d_{Pt} from TEM is not possible. We can, however, estimate it by subtracting the peak height of the roughness profiles from the Pt layer thickness D_{Pt} measured far from the sample border, i.e., where the TEM section is thicker but quite uniform. The same value is to be added to the C-layer thickness. More precisely:

$$d_{\mathrm{Pt}} = D_{\mathrm{Pt}} - \sqrt{2}(\sigma_{\mathrm{Pt}} + \sigma_{\mathrm{C}}),$$

$$d_{\mathrm{C}} = D_{\mathrm{C}} + \sqrt{2}(\sigma_{\mathrm{Pt}} + \sigma_{\mathrm{C}}).$$

The sum of the two rms roughnesses takes into account the apparent increase or decrease of the layer from both sides,

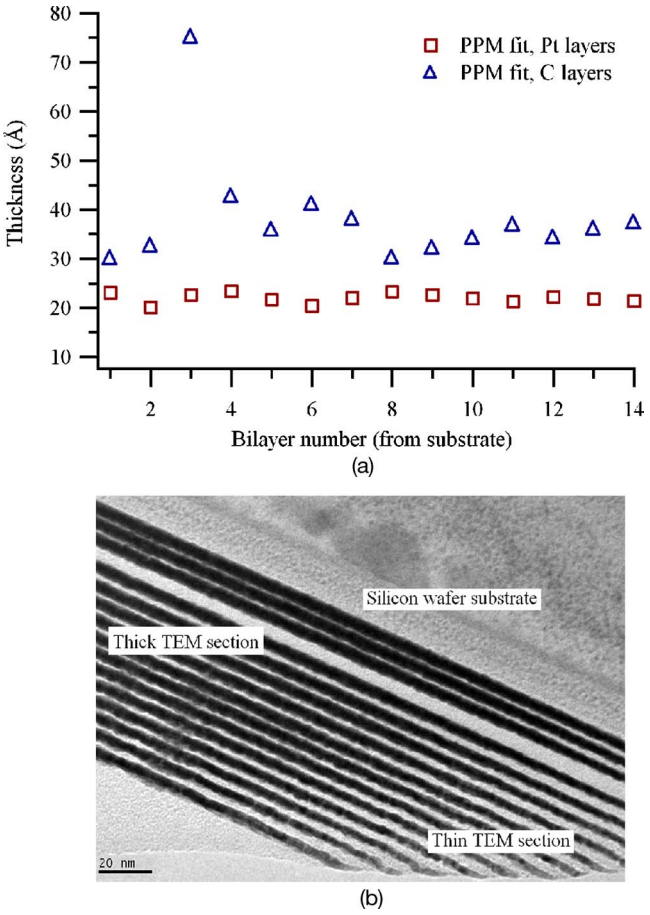

Fig. 3 (a) The Pt and C thickness trends as obtained by PPM. Irregularities in the *d* spacing are mainly caused by C layers (the third one in particular), whereas Pt layers are more regular. (b) TEM section of the Pt/C sample; the dark bands are the Pt layers; the white ones are the C layers. The growth direction is from the top down in the image. The layer thickness appears to be a function of the section thickness as an effect of the superposition of Pt layer roughness topographies; thus, the PPM results should be compared with the TEM results at the border of the sample. Notice the exceptional thickness of the third C layer, caused by an instability in the e-beam gun used to evaporate the sample.

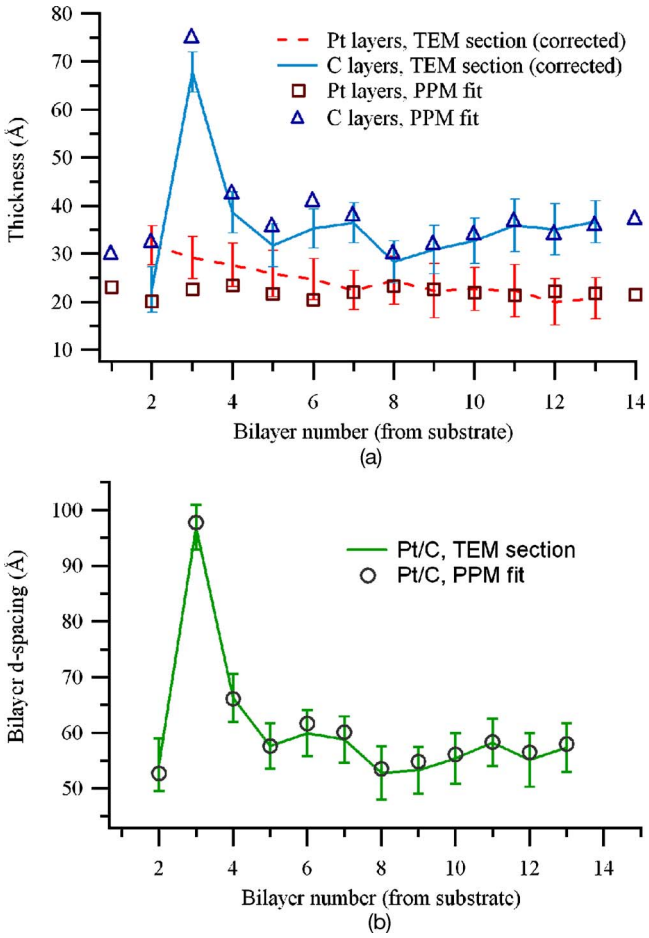

Fig. 4 (a) Comparison of PPM (plotted points) and TEM (lines) results after removal of the roughness effect from the TEM results. The TEM results are obtained from the average of 11 equally spaced profiles of the TEM section. Notice the symmetry of the discrepancies, which are due to a nonuniform projected roughness. The TEM error bars mark the 1σ confidence interval: the error bars include the intrinsic TEM resolution and the thickness variation of the 11 profiles. (b) Bilayer *d*-spacing distribution as calculated by PPM for the scan at 8.05 keV. Uncorrected *d*-spacing values are in agreement with the thickness values derived from the TEM analysis within 1.6 Å, i.e., well inside the TEM confidence interval.

and the factor $\sqrt{2}$ is the ratio of peak value to rms. With the Pt and C rms roughnesses found from the fit (5.2 and 4.3 Å) we concluded that the TEM measurements of the Pt layers must be reduced by 13.5 Å and those of the C layers increased by the same amount. The comparison of the code predictions with the corrected TEM results is presented in Fig. 4(a). The agreement is satisfactory.

It should be noted that the residual discrepancy (first and last bilayers) may be due to the nonuniform thickness of the TEM section. The first layers are more distant from the sample border than the last ones. This enhances the projection effect in the first bilayers; hence the correction there has probably been underestimated. Note as well that in this particular case the roughness growth detected by PPM (from 3 to 5.2 Å) could have partially compensated the projection effect reduction in the last bilayers caused by the thickness decrease in the TEM sample.

A further confirmation of that comes from the bilayer *d*-spacing distribution, which should not be affected by this correction, since the corrections for Pt and C have opposite sign and cancel out when they are summed to compute the bilayer *d* spacing. The comparison of the bilayer *d* spacing as determined via TEM and through the PPM analysis is shown in Fig. 4(b). The very good agreement is apparent.

4.2 Ni/C *Sample*

The Ni/C multilayer (19 bilayers) stack was modeled following a similar computational scheme to that for the Pt/C multilayer. All layer thickness values can vary independently. The Ni and C densities were kept constant (the assumed density of Ni was 8.7 g/cm^3, and that of C 1.6 g/cm^3). The roughness values are kept constant within six blocks of three bilayers (except the last one, which had four bilayers); however, the roughness of each block can be varied in order to allow for a roughness drift through the stack. The first C layer was ignored because the density contrast with the Si wafer is negligible.

The model structure has been optimized to match simultaneously the reflectivity curves at both photon energies, 8.05 and 17.45 keV. The initial thickness values were 30 Å for Ni and 100 Å for C; the Ni layers were left free to vary between 30 and 50 Å, and the C layers between 70 and 120 Å. For the entire computation to be accomplished, 2 h 10 min of CPU time was needed. The model-experiment agreement is evident (see Fig. 5). The reflectance features are now fitted accurately. The logarithmic χ^2 is 7.26 at 8.05 keV and 10.6 at 17.45 keV. The corresponding χ^2_ν are 0.025 at 8.05 keV and 0.067 at 17.45 keV.

The main result of this two-energy-scan fit can be summarized as follows: The rms roughness drifts from 3.0 to 3.9 Å for both Ni and C, on going from the substrate to the multilayer outer surface; the Ni and C layer thickness distribution shows [see Fig. 6(a)] a slight thickness variation of the Ni layers (a few angstroms) and a very large thickness variation of the C layers. The overall thickness drift originates from the imperfect deposition of the C layers. The total *d*-spacing variation over the entire stack is 2 nm.

The layer thickness distribution [Fig. 6(a)] has been compared with the data worked out from the TEM section of the same multilayer [Fig. 6(b)]. Figure 7(a) displays the comparison between the PPM results and the TEM data, corrected for the roughness projection; in this case the correction amounts to 12 Å, assuming the maximum roughness value inferred by PPM. The agreement seems to be good only for the first bilayers, for the others the required roughness is much larger than the measured one. This can be explained by observing that the TEM sample is thicker in the image upper part [this can be seen from the image darkening in Fig. 6(b)]. The growth direction is from the bottom to the top of the image; thus both the thickening and roughness growths contribute to the apparent increase of the Ni layers' thickness as the distance from the substrate increases. The thicker the specimen to be crossed by the electron beam, the stronger the shadow effect of the projected interface roughness. This effect may have been enhanced by the fact that, due to the imaging conditions, the beam could not be parallel to the interface planes.

The agreement between PPM and TEM is, instead, very satisfactory when we compare the bilayer *d*-spacing values [see Fig. 7(b)], which are not affected by the roughness

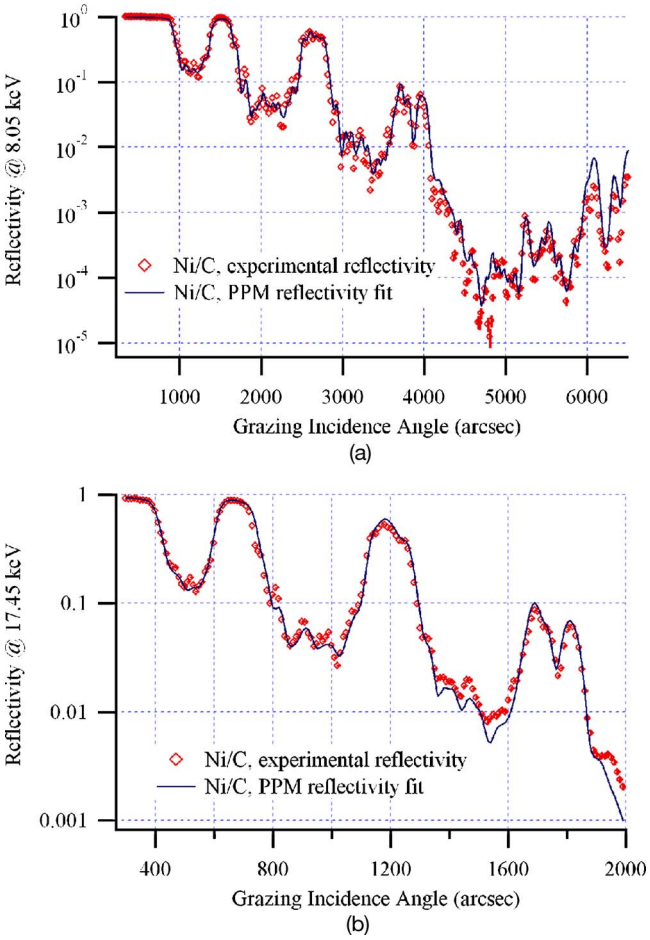

Fig. 5 The reflectivity at (a) 8.05 keV and (b) 17.47 keV of the Ni/C multilayer sample compared with the PPM fitted model (log scale). The two scans (8.05 and 17.45 keV) were processed simultaneously. Error bars (very small) are also included.

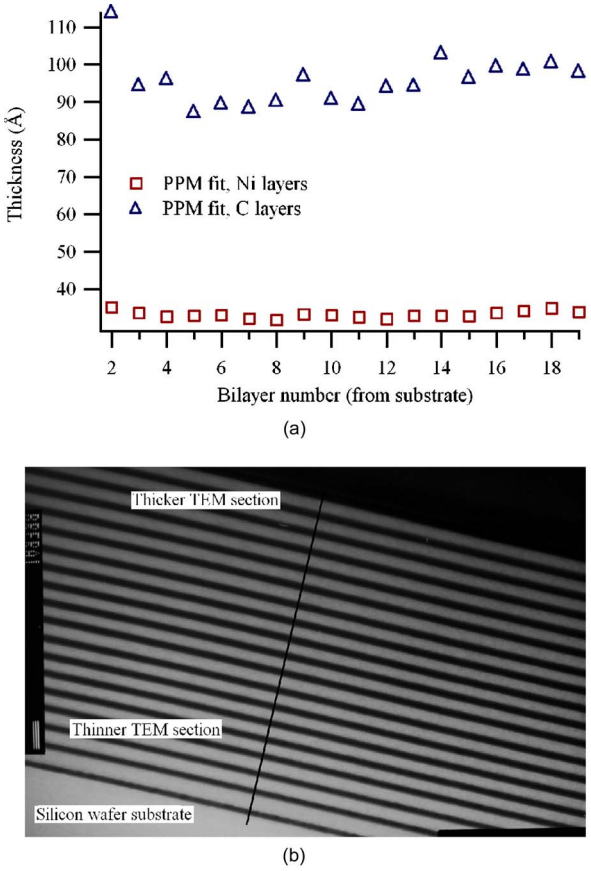

Fig. 6 (a) The Ni/C layer thickness distribution as generated by PPM. Irregularities of the *d* spacing are mainly caused by C layers. The same result was obtained in a previous work, with the stack modeled as a sequence of blocks: the short-period variation could not be seen in that case. (b) The TEM section of the Ni/C multilayer. The Ni layers are the dark bands; the C layers are the bright bands; the growth direction is from the bottom up. The length of the black marker is 219 nm.

shading effect. This result confirms the correctness of the PPM prediction and the interpretation of the TEM profiles.

4.3 W/Si *Sample*

For the W/Si sample (40 bilayers) the number of free parameters would be too large to converge quickly to the global minimum if we allowed the thickness of each layer to vary freely. The fitting strategy was changed as follows: the W and Si layer thicknesses were initially allowed to drift throughout the stack; we adopted a second-order polynomial law for the layer thickness distribution, the coefficients of which were optimized to fit the experimental XRR curves. The initial structure was set to be a periodic one, with 16 Å for the W layers and 38 Å for the Si layers as guess values. In this case, single-layer calibrations were not allowed, while the densities were set free to vary in the range 16 to 19.5 g/cm^3 for W and 1.8 to 3.0 g/cm^3 for Si, starting from natural density values (19.3 and 2.3 g/cm^3, respectively). In order to account for a roughness growth in the stack, the roughness rms was supposed to be varying, following a second-order polynomial law.

The structure optimization process was run at both 8.05 and 17.45 keV. After 30 min, the main reflectance peaks were well fitted but most features could not be explained by assuming a continuous drift. In order to improve the fit quality we removed the power-law constraint, leaving each layer free to vary independently within a 4-Å-wide interval around the values found in the previous step. The density and roughness values were still allowed to move in the same intervals. The optimization was restarted several times, each time changing the upper and the lower bound of each thickness whenever the value derived from the fit came too close to one of the bounds. Following this method, we could gradually find the thickness distribution remaining in the initial interval of variability of the parameters.

After 5 h of CPU time the optimization was accomplished, yielding a solution that matches well the reflectivity at 8.05 keV at all angles [see Fig. 8(a)] and at 17.45 keV except at angles near 1900 and 3000 arcsec [Fig. 8(b)]; this discrepancy might have been caused by imperfect energy filtering of the x-ray beam in the experimental setup when measuring the reflectivity of this sample. The beam polychromaticity should not, however, exceed 1% of the intensity of the 17.45-keV line, so that the PPM results ought not to be significantly altered. The logarithmic χ^2 is 12.5 at 8.05 keV and 1.32 at 17.45 keV, and the corre-

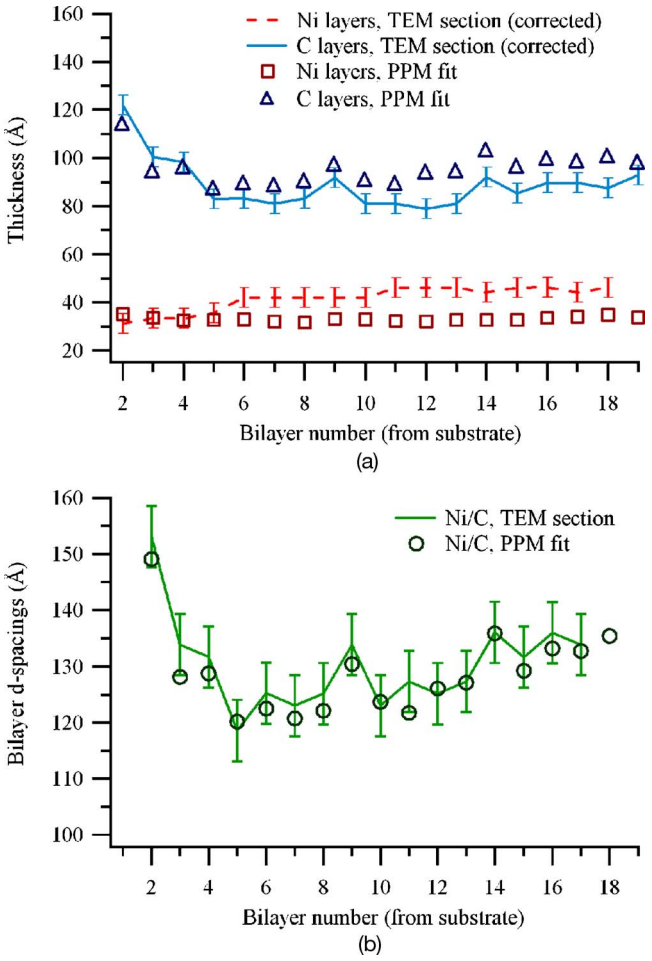

Fig. 7 (a) Comparison between TEM (lines) and PPM (marks) results for the Ni and C thickness distributions. Although the trends are similar (notice the matching of peaks in the C layers), the discrepancy is larger at the multilayer surface, as a likely consequence of the roughness and section-thickness increases. Thickness measurements on the last Ni and the first C layer were not possible. (b) The bilayer *d*-spacing distribution in the multilayer as found from the PPM optimization. The data match is very good.

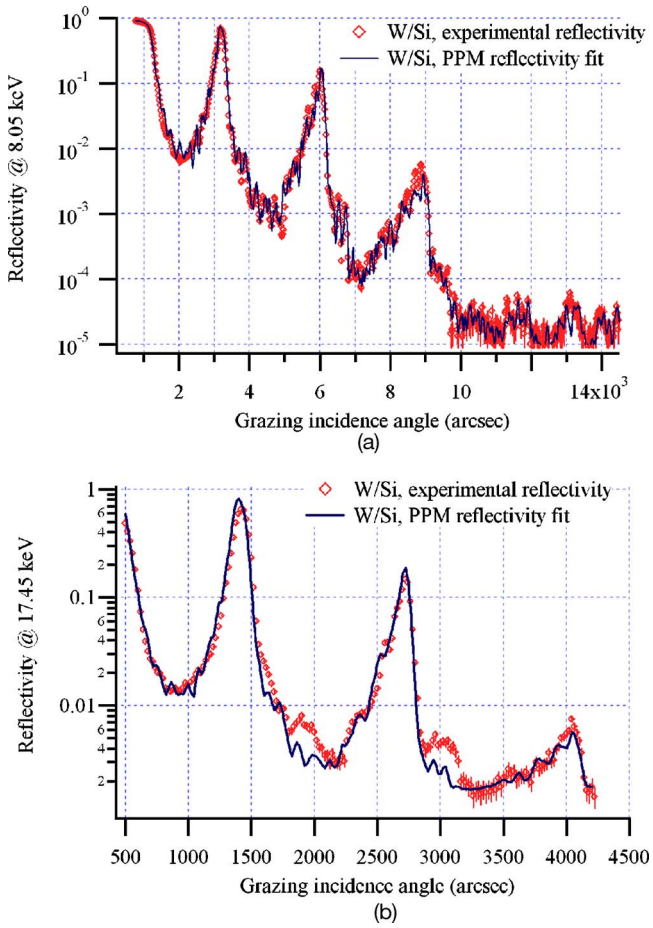

Fig. 8 The reflectivity at (a) 8.05 keV and (b) at 17.45 keV of the W/Si multilayer sample compared with the PPM model predictions after allowing for individual thickness variations (log scale). The fit was executed simultaneously on both scans.

sponding χ^2_ν values are 0.020 at 8.05 keV and 0.015 at 17.45 keV. The multilayer stack structure inferred from the fit is shown in Fig. 9(a). Both long-range drift and rapid variations of the thickness are present. In particular, the Si layers exhibit a pronounced decrease.

The calculated Si density (2.2 g/cm^3) is close to the natural one (2.3 g/cm^3), whereas the calculated W density (16.3 g/cm^3) is 15% smaller than the natural one (19.2 g/cm^3). A reduction of density in thin W films was already observed (17.4 g/cm^3) by Levine et al.[35] They also report[36] that sometimes the W density value can be smaller even by factor of 2. Within the limits of the resolution of our instrument, TEM investigations have not revealed porosity of the samples on the scale of nanometers, but the analyses were complicated by the noncrystalline structure of the layers. Higher-resolution techniques are needed to detect porosity at lower scale. The same consideration applies to the low density of C reported in Sec. 4.1. The analysis with PPM provided clear evidence of roughness growth in the stack, from 3.1 to 4.8 Å, going from the substrate to the multilayer surface.

The *d*-spacing variation of this sample is less evident than for the previous samples. Also in this case the roughness projection effect is present, as one can easily see by observing the thickness reduction of the W layers in the magnified image [Fig. 9(b)]. Since the thickness gradient in this case is approximately perpendicular to the growth direction, we can allow for the roughness when inspecting the thickness distribution from the TEM image (averaged over 30 equally spaced profiles in order to suppress local undulations of the interfaces), applying the equations reported in Sec. 4.1, where the σ values used to compute the correction vary according to the trend predicted by PPM. The TEM layer thicknesses after correction and the PPM results are compared in Fig. 10(a). The agreement is apparent.

Figure 10(b) shows also the comparison of the *d*-spacing values. As already mentioned, the *d*-spacing distribution derived from TEM is not affected by the roughness projection effect, since only the Γ factor is altered by the roughness in the TEM image. The PPM and TEM findings are in very good agreement.

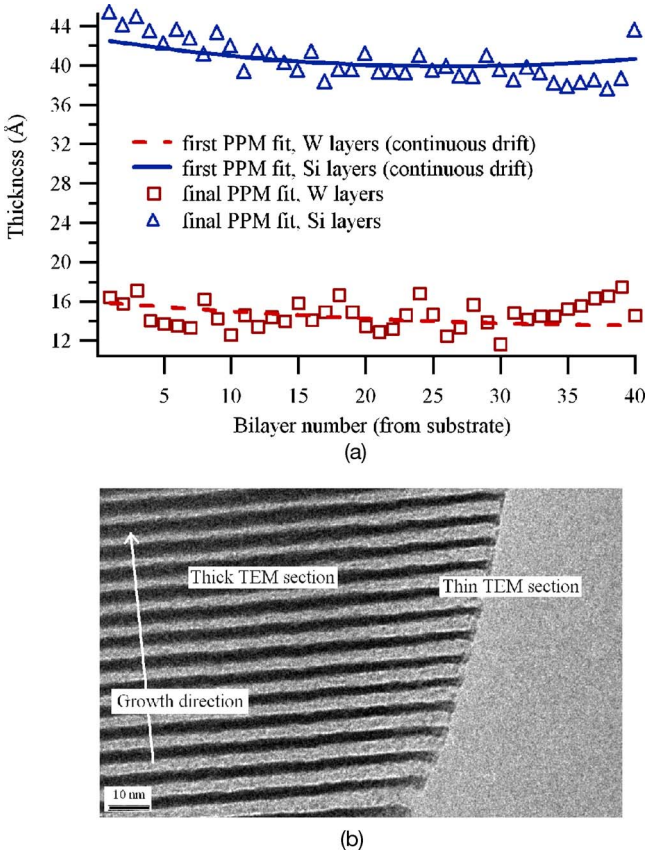

Fig. 9 (a) The W and Si thickness distribution as derived by PPM (plotted points). The layer drifts found in the first step of the fit are also plotted (lines). (b) The TEM sample close to the edge: The roughness projection effect is clearly seen.

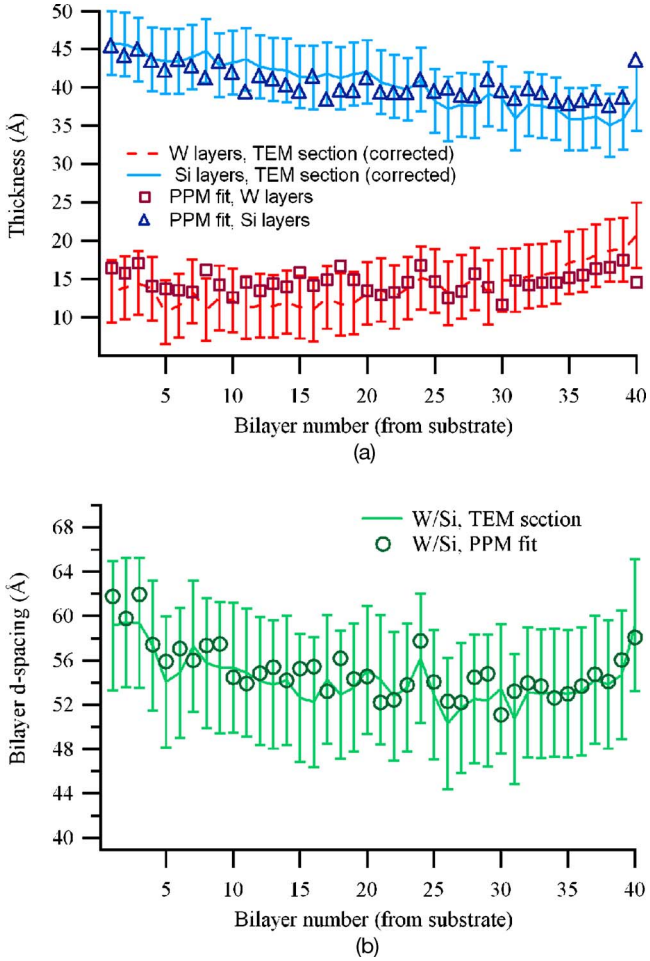

Fig. 10 (a) Comparison of PPM (plotted points) and TEM (lines) results after removal of the roughness TEM artifact. The TEM results are obtained from averaging 30 equally spaced TEM section profiles. The TEM error bars mark the 1σ confidence interval. (b) Bilayer *d*-spacing comparison. The agreement is very good.

5 Summary

The high sensitivity of the XRR to small variations of the individual layer thickness and roughness in a multilayer and the ability of PPM to handle the large number of stack parameters makes the analysis of XRR with PPM a powerful and nondestructive tool for the deep characterization of layered coatings with period in the nanometer range. The fitting capabilities of PPM have been tested and validated for two quasiperiodic multilayer samples (Pt/C and Ni/C) with significant *d*-spacing irregularities. High-quality fit results were obtained for x-ray reflectance curves at two photon energies simultaneously. The calculated *d*-spacing distributions are in good agreement with the corresponding TEM data. The comparison shows, moreover, that the multilayer Γ ratio can be altered in TEM images by geometrical effects like the superposition of the multilayer roughness profiles in the image plane. Because the XRR analysis is not affected by image artifacts, we have been able to extract with a large accuracy the actual layer thickness distribution in the multilayer stack.

Future developments will be aimed to using PPM for XRR scans of multilayers deposited via other techniques (e.g., RF magnetron sputtering) and/or with a larger number of bilayers, especially graded multilayers for wideband x-ray reflectivity. The comparison of the related results with TEM images will cast some light on the reliability of PPM as a diagnostic tool for multilayers with various applications.

Acknowledgments

The authors gratefully acknowledge the support of O. Citterio, T. Maccacaro (INAF/Osservatorio Astronomico di Brera), G. Nocerino (Media Lario Technologies, Bosisio Parini, Italy) for this work. They thank L. Pina (Reflex s.r.o., Prague, Czech Republic) for providing them with the W/Si sample. D. Spiga is indebted to the Italian Ministry for Universities for a COFIN grant addressed to the development of multilayer coatings for x-ray telescopes, and to the European Science Foundation (COST Cooperation, Action P7) for the grant that made the PPM training at the ESRF possible. He thanks especially T. Krist (Hahn-Meitner Institut, Germany) and M. Idir (Synchrotron Soleil, France) for their support. The valuable collaboration of G. Valsecchi, G. Grisoni, M. Cassanelli (Media Lario Technologies) is gratefully acknowledged. V. Cotroneo is grateful to the Cariplo Foundation for the grant funding his fellowship. PPM is open-source

software; it can be freely downloaded from ftp://www.esrf.fr/pub/scisoft/ESRF_sw/linux_i386_03/

References

1. F. Fiore, G. Perola, G. Pareschi, O. Citterio, A. Anselmi, and A. Comastri, "HEXIT-SAT: a mission concept for x-ray grazing incidence telescopes from 0.5 to 70 keV," *Proc. SPIE* **5488**, 933–943 (2004).
2. S. Romaine, S. Basso, R. Bruni, W. Burkert, O. Citterio, G. Conti, D. Engelhaupt, M. Freyberg, M. Ghigo, P. Gorenstein, M. Gubarev, G. Hartner, F. Mazzoleni, S. O'Dell, G. Pareschi, B. Ramsey, C. Speegle, and D. Spiga, "Development of a prototype nickel optic for the Constellation-X hard x-ray telescope: III," *Proc. SPIE* **5900**, 225–231 (2005).
3. G. Pareschi and V. Cotroneo, "Soft (0.1–10 keV) and hard (>10 keV) x-ray multilayer mirrors for the XEUS astronomical mission," *Proc. SPIE* **5168**, 53–64 (2004).
4. P. Ferrando, "SIMBOL-X: a new generation x-ray telescope," *Proc. SPIE* **5168**, 65–76 (2004).
5. K. D. Joensen, P. Voutov, A. Szentgyorgyi, J. Roll, P. Gorenstein, P. Høghøj, and F. E. Christensen, "Design of grazing-incidence multilayer supermirrors for hard x-ray telescopes," *Appl. Opt.* **34**(34), 7934–7945 (1995).
6. Y. Tawara, K. Yamashita, H. Kunieda, K. Tamura, A. Furuzawa, K. Haga, N. Nakajo, T. Okajima, H. Takata, et al., "Development of a multilayer supermirror for hard x-ray telescopes," *Proc. SPIE* **3444**, 569–575 (1998).
7. L. G. Parrat, "Surface studies of solids by reflection of x-rays," *Phys. Rev.* **95**(2), 359–369 (1954).
8. F. Abelès, "Recherche sur la propagation des ondes électromagnétiques sinusoïdales dans les milieux stratifiés," *Ann. Phys. (Paris)* **127**, 597 (1950).
9. D. G. Stearns, "The scattering of x-rays from non-ideal multilayer structures," *J. Appl. Phys.* **65**, 491–506 (1989).
10. L. Nevot and P. Croce, "Caracterisation des surface par reflexion rasante de rayons x. Application à l'étude du polissage de quelques verres silicates," *Rev. Phys. Appl.* **15**, 761–779 (1980).
11. M. Sanchez del Rio and R. J. Dejus, "Status of XOP: an x-ray optics software toolkit," *Proc. SPIE* **5536**, 171–174 (2004).
12. D. L. Windt, "IMD: software for modeling the optical properties of multilayer films," *Comput. Phys.* **12**, 360–370 (1998).
13. M. Wormington, C. Panaccione, K. M. Matney, and D. K. Bowen, "Characterization of structures from x-ray scattering data using genetic algorithms," *Philos. Trans. R. Soc. London* **357**, 2827–2848 (1999).
14. M. Sanchez del Rio and G. Pareschi, "Global optimization and reflectivity data fitting for x-ray multilayer mirrors by means of genetic algorithms," *Proc. SPIE* **4145**, 88–96 (2001).
15. D. Šimek, D. Rafaja, and J. Kub, "Genetic algorithm applied to multilayer structure determination," *Krystalograf. společnost Mater. Structure* **8**(1), 16–21 (2001).
16. V. Cotroneo and G. Pareschi, "Global optimization of x-ray astronomical multilayer mirrors by an iterated simplex procedure," *Proc. SPIE* **5536**, 49–60 (2004).
17. E. Ziegler, C. Morawe, I. V. Kozhevnikov, T. Bigault, C. Ferrero, and A. Tallandier, "Wide-band multilayer mirrors for medium to hard x-ray applications," *Proc. SPIE* **4782**, 169–175 (2002).
18. S. D. Brown, L. Bouchenoire, A. Mirone, and V. Cotroneo, "Progress report on XmaS U/Fes multilayer measurement and analysis," Report, European Synchrotron Radiation Facility (2004).
19. J. A. Nelder and R. Mead, "A simplex method for function minimization," *Comput. J.* **7**(4), 308–313 (1965).
20. N. A. Metropolis, A. W. Rosenbluth, M. N. Rosenbluth, A. Teller, and E. Teller, "Equation of state calculations by fast computing machines," *J. Chem. Phys.* **21**(6), 1087–1092 (1953).
21. S. Kirkpatrick, C. D. Gelatt, and M. P. Vecchi, "Optimization by simulated annealing," *Science* **220**, 671–680 (1983).
22. V. Cerny, "A thermodynamical approach to the travelling salesman problem: an efficient simulation algorithm," Report, Comenius Univ., Bratislava, Slovakia (1982).
23. E. Ziegler, C. Ferrero, F. Lamy, C. Chapron, and C. Morawe, "Characterisation of nanometer layered structures using multiple wavelength x-ray reflectometry and simulated annealing data analysis," in *Adv. X-Ray Anal.* **45**, 45–54, ICDD (2002).
24. O. Citterio, G. Bonelli, G. Conti, E. Mattaini, E. Santambrogio, B. Sacco, E. Lanzara, H. Brauninger, and W. Burkert, "Optics for the x-ray imaging concentrators aboard the x-ray astronomy satellite SAX," *Appl. Opt.* **27**(8), 1470 (1988).
25. P. Gondoin, B. Aschenbach, M. W. Beijersbergen, R. Egger, F. A. Jansen, Y. Stockman, and J. P. Tock, "Calibration of the first XMM flight mirror module: I—image quality," *Proc. SPIE* **3444**, 278–289 (1998).
26. D. N. Burrows, J. E. Hill, J. A. Nousek, A. A. Wells, A. D. Short, R. Willingale, O. Citterio, G. Chincarini, and G. Tagliaferri, "Swift x-ray telescope," *Proc. SPIE* **4140**, 64–75 (2000).
27. D. Spiga, G. Pareschi, O. Citterio, R. Banham, M. Cassanelli, V. Cotroneo, G. Grisoni, B. Negri, G. Valsecchi, and D. Vernani, "Development of multilayer coatings (Ni/C–Pt/C) for hard x-ray telescopes by e-beam evaporation with ion assistance," *Proc. SPIE* **5488**, 813–819 (2004).
28. D. Spiga, G. Pareschi, G. Grisoni, and G. Valsecchi, "Hard x-ray multilayer coated astronomical mirrors by e-beam deposition," *Proc. SPIE* **5533**, 66–74 (2004).
29. Center for X-Ray Optics, http://www-cxro.lbl.gov/cgi-bin/mldata.pl.
30. F. H. Fabreguette, R. A. Wind, and S. M. George, "Ultrahigh x-ray reflectivity from W/Al_2O_3 multilayers fabricated using atomic layer deposition," *Appl. Phys. Lett.* **88**, 013116 (2006).
31. S. Muhl, E. Camps, L. Escobar-Alarcón, and O. Olea, "Electron evaporation of carbon using a high density plasma," *Thin Solid Films* **373**, 255–260 (2000).
32. G. Pareschi, O. Citterio, S. Basso, M. Ghigo, F. Mazzoleni, D. Spiga, W. Burkert, M. Freyberg, G. D. Hartner, G. Conti, E. Mattaini, G. Grisoni, G. Valsecchi, B. Negri, G. Parodi, A. Marzorati, and P. dell'Acqua, "Development of grazing-incidence multilayer mirrors by direct Ni electroforming replication: a status report," *Proc. SPIE* **5900**, 47–58 (2005).
33. D. Spiga, A. Mirone, C. Ferrero, V. Cotroneo, G. Pareschi, M. Sanchez del Rio, and D. Vernani, "Fitting x-ray multilayer reflectivities by means of the PPM code," *Proc. SPIE* **5536**, 71–80 (2004).
34. D. Spiga, A. Mirone, G. Pareschi, R. Canestrari, V. Cotroneo, C. Ferrari, C. Ferrero, L. Lazzarini, and D. Vernani, "Characterization of multilayer stack parameters from x-ray reflectivity data using the PPM program: measurements and comparison with TEM results," *Proc. SPIE* **6266**, 346–357 (2006).
35. Z. H. Levine, S. Grantham, and I. McNulty, "Mass absorption coefficient of tungsten for 1600–2100 eV," *Phys. Rev. B* **65**, 064111 (2002).
36. L. I. Maissel and M. H. Francombe, *An Introduction to Thin Films*, pp. 117–118, Gordon and Breach (1973).

Daniele Spiga received his master's degree in physics at the University of Milan in 2000 with a thesis in radio astronomy. He received a PhD in astronomy and astrophysics in 2005 with a thesis on the development of multilayer-coated mirrors for x-ray telescopes. This thesis was awarded the Pietro Tacchini Prize of the SAIT (the Italian Astronomical Society). He is now working at INAF/Osservatorio Astronomico di Brera, on the theoretical and experimental study of the focusing and imaging performance of multilayer-coated optics.

Giovanni Pareschi received his master's degree in astronomy in 1992 at the University of Bologna (Italy), and his PhD in physics in 1996 at the University of Ferrara (Italy). From 1997 to 1998 he was an ESA postdoctral fellow at the Danish Space Research Center of Copenhagen (Denmark). Since 1999 he has been an associate astronomer with INAF/Osservatorio Astronomico di Brera (Merate, Italy). He is presently a project scientist of the SIMBOL-X mission. His main field of interest is the development, implementation, and calibration of x-ray optics for astronomical missions.

Vincenzo Cotroneo received his master's degree in physics in 2003 at the University of Milan with a thesis on "Multilayer optimisation for hard x-ray optics." He has been working with the X-ray Technology Group at INAF/Osservatorio Astronomico di Brera, dealing with the optimization and simulation of astronomical multilayer-coated mirrors and related software development. Presently he is a PhD student at the same university, preparing a thesis on "Design and development of x-ray optics for astronomical missions." In 2004 he spent one month at the ESRF (Grenoble, France) as a visiting junior scientist.

Rodolfo Canestrari received his master's degree in astronomy in 2006 at the University of Bologna (Italy) with a thesis, "Hard x-ray astronomical telescopes: technological development of multilayer-coated mirrors", carried out at INAF/Osservatorio Astronomico di Brera (Italy). He works on hard-x-ray multilayered mirrors for future telescopes and on the hot slumping technique for a new generation of ground-based telescopes (ELT class).

Dervis Vernani received his master's degree in astronomy at the University of Bologna (Italy) in 2004 with the thesis "Multilayered mirrors for hard x-ray imaging astronomical telescopes," for which he did the research at the INAF/Osservatorio Astronomico di Brera (Italy). He continued working in the same lab with the X-ray Technology Group, dealing with XRR measurements and reflectivity simulation of multilayered mirrors. He is presently working in the R&D Department of Media Lario Technologies (Lecco, Italy) on optical devices for future x-ray astronomy missions.

Alessandro Mirone: Biography and photograph not available.

Claudio Ferrero graduated from the Politecnico of Turin in the Faculty of Nuclear Engineering. He received his PhD on a topic in nuclear reactor safety at the University of Karlsruhe. After a period spent at the research center of Karlsruhe as a research staff member working initially in the area of computer-aided geometric design and later dealing with the modeling of fusion materials under neutron irradiation, he joined the European Synchrotron Radiation Facility (ESRF), where he was appointed the head of the Scientific Software Service in 2001. His research interests include x-ray optics, x-ray dynamical diffraction theory, soft condensed matter and porous materials studied by small-angle x-ray scattering, and x-ray microtomography.

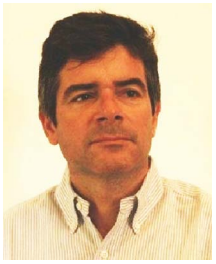

Claudio Ferrari has been a senior researcher since 2001 at IMEM (Institute of Materials Science for Electromagnetic Applications), which is associated with the Italian National Research Council. His research activities cover the study of single-crystal components for x-ray optics and the characterization of semiconductor heterostructures by x-ray techniques. He is presently leading a group in charge of studying materials and preparing devices for energy production, such as solar cells and high-temperature superconductors.

Laura Lazzarini has been a staff researcher at the Institute of Magnetic and Electronic Materials of the Italian National Council of Research since 1994. She has wide experience in transmission and scanning electron microscopy and cathodoluminescence, mainly applied to semiconducting materials. She is currently involved in the development and application of experimental techniques with nanometric lateral resolution to the study of systems for opto- and nanoelectronic applications, and in the correlation between the structural and optical properties of the materials.